



Biogenic Photodegradation of Methylene Blue Dye using *Azadirachta Indica* (Neem) Leaf Extract: A Novel Green Catalyst Approach

K. Suba¹, V. Padmavathy², S. R. Anishia³, S. Malini⁴, R. Kavitha⁵ and S. Sasikruba^{6*}

¹Department of Chemistry, Sri Sairam Engineering College, Chennai, TN, India

²Department of Physics, Prathyusha Engineering College, Tiruvallur, TN, India

³Department of Physics, Tagore Engineering College, Chennai, TN, India

⁴Department of Physics, Sengamala Thayaar Educational Trust Women's College, Mannargudi, Thiruvarur, TN, India

⁵Department of Physics, Rajalakshmi Institute of Technology, Chennai, TN, India

⁶Department of Chemistry, RRASE College of Engineering, Chennai, TN, India

Received: 28.10.2024 Accepted: 17.12.2024 Published: 30.12.2024

*sasitharunika@gmail.com

ABSTRACT

This study reports the green synthesis of zinc oxide (ZnO) nanoparticles using *Azadirachta Indica* (neem) leaf extract (AIL), providing an environmentally sustainable approach for environmental and biomedical applications. Neem leaves were thoroughly washed, air-dried, and ground into a fine powder, which was then used to prepare an aqueous extract. ZnO nanoparticles were synthesized by reacting zinc sulphate and sodium hydroxide solutions, to which neem extract was added dropwise. The reaction mixture was then subjected to drying and annealing, resulting in the formation of ZnO nanoparticles. Characterization through scanning electron microscopy (SEM), Fourier-transform infrared spectroscopy (FTIR), X-ray diffraction (XRD), and Brunauer-Emmett-Teller (BET) analysis demonstrated enhanced dispersion, bio-functionalization, high crystallinity, and an increased surface area. The AIL/ZnO nanoparticles demonstrated superior photocatalytic activity, achieving complete degradation of methylene blue dye at pH 7. Additionally, they exhibited potent antimicrobial activity against both Gram-positive and Gram-negative bacteria. This environmentally friendly synthesis approach minimizes the use of hazardous chemicals and yields multifunctional nanoparticles with significant potential for wastewater treatment and antimicrobial applications, positioning AIL/ZnO as a promising material for addressing environmental and healthcare challenges.

Keywords: *Azadirachta Indica*; ZnO; Methylene blue (MB); Photodegradation.

1. INTRODUCTION

The environmental implications of colorant pollution have garnered significant attention in recent decades. Industries such as textile, leather, paper, plastics, and pharmaceuticals are major contributors to the generation of dye-contaminated wastewater on a global scale (Bairwa *et al.* 2024). Azo compounds, comprising 60–70% of dyes in textile wastewater, are resistant to degradation and significantly contribute to water pollution, posing environmental challenges (Algarni *et al.* 2022). Water, the main component of Earth's rivers, lakes, and seas, is a tasteless, odorless, nearly colorless substance essential to life. A universal solvent, it facilitates countless biological and chemical processes despite lacking calories or nutrients (Rekha *et al.* 2021). Industrial wastewater is a major environmental concern due to its harmful impact on both human health and aquatic ecosystems. Contaminants present in industrial effluents, such as heavy metals, organic pollutants, and dyes, can lead to severe health issues, including toxicity and chronic diseases. Additionally,

these pollutants disrupt aquatic habitats by altering water quality, reducing biodiversity, and affecting the ecological balance (Qasim *et al.* 2024). Hazardous slurries are utilized in conventional industries for the fabrication and polishing of high-performance components, particularly in the semiconductor, microelectronics, and aerospace sectors. Significant focus has been placed on nanomaterials research due to their exceptional physical and chemical properties. Nanomaterials exist in various forms, including nanoparticles, nanorods, and nanowires. Metal oxides, recognized for their non-toxicity and natural abundance, exhibit a high surface area at the nanoscale, coupled with notable chemical and thermal stability (Hessien *et al.* 2021). Science and technology have made rapid advancements in the development of green technologies. The term "nanomaterial" refers to materials with at least one dimension in the range of 1 to 100 nm, exhibiting unique properties such as altered porosity, morphology, size, and enhanced functionalities (Ashour *et al.* 2023). Plant systems are efficient at converting light energy into chemical energy and are capable of uptaking,

accumulating, utilizing, and recycling various mineral species. As such, plants and their derivatives serve as an excellent source of renewable and sustainable materials for nanoparticle synthesis.

Plant-based methods utilizing aqueous extracts operate under ambient temperature and atmospheric pressure, facilitating the production of highly stable nanoparticles. This approach allows for rapid and cost-effective bulk production (Oza *et al.* 2020). To mitigate this issue, green synthesis methods for nanoparticles, nanomaterials, and nanotechnology are being employed to develop innovative, environmentally-friendly slurries. (Karvekar *et al.* 2022). The field of "green" chemistry emerged in the United States during the 1990s. European countries have since enacted some of the most advanced regulations concerning "green" technologies (Soltys *et al.* 2021). Green synthesis is a cost-effective, environmentally friendly method that avoids the use of harmful chemicals, making it a sustainable alternative to traditional synthesis routes. The use of plant extracts as a green synthesis technique is considered the most reliable, as it ensures the production of biocompatible, non-toxic, and eco-friendly nanoparticles. This approach leverages the natural ability of plants to reduce and stabilize metal ions, offering a safer, more sustainable route for nanoparticle fabrication without compromising efficiency or stability (Alqarni *et al.* 2022).

The newly synthesized *Azadirachta Indica* Leaves/ZnO nanoparticles not only facilitate the removal of dyes from industrial wastewater but also inhibit bacterial growth, contributing to water purification. The biomolecules present in the plant extracts act as capping agents around the nanoparticles, enhancing their stability and making them medicinally valuable. Numerous studies in the literature report that these plant-extract-derived materials exhibit a range of applications in medicine due to the formation of less toxic or non-toxic nanomaterials (Ravikumar *et al.* 2022). The plant extract-mediated green synthesis of metal oxide nanoparticles (MONPs) has garnered significant attention due to the diverse phytochemicals found in various parts of plants, such as nimbin, nimbolinin, nimbidol, nimbidin, gedunin, sodium nimbin, quercetin, and salannin, which are reported in different parts of the neem tree. The bioactive compounds in *Azadirachta Indica* extract, such as nimbin, nimbolinin, gedunin, and quercetin, which play key roles in stabilizing and enhancing ZnO nanoparticles. These compounds act as reducing agents for nanoparticle formation and stabilizing agents to prevent agglomeration. Additionally, they improve the antimicrobial and photocatalytic properties of the nanoparticles, contributing to their effectiveness in applications like dye degradation and antimicrobial treatments. These phytochemicals serve as both reducing and stabilizing agents simultaneously. Gedunin, a key limonoid predominantly found in the seeds of plants within the Meliaceae family, plays a crucial role in this

process. In this novel approach, a single plant extract serves both as the reducing and stabilizing agent, eliminating the need for separate reductants and stabilizers in typical reactions (Martin *et al.* 2023). Additionally, water was employed as a solvent instead of organic solvents in the nanoparticle synthesis process. In this study, three types of dyes, including methylene blue (MB) and thiazine dye, were selected to evaluate and compare the catalytic performance of the as-synthesized materials. The degradation of the dyes reached 100% within 15 to 22 minutes (Sahin *et al.* 2022). The biomolecules in plant extracts act as capping agents around nanoparticles, enhancing their stability and medicinal properties. Numerous studies have highlighted the potential of these plant-synthesized nanoparticles in medicine due to their reduced toxicity or non-toxic nature. This study aims to synthesize zinc oxide (ZnO) nanoparticles using *Azadirachta Indica* leaf extract and to characterize their antibacterial, antimicrobial, and photocatalytic properties.

The research focuses on evaluating the effectiveness of these ZnO nanoparticles in various biomedical and environmental applications (Kavya *et al.* 2023). Recent studies have focused on investigating the antimicrobial activity and multifunctional properties of various nanoparticles (NPs) and nanocomposites (NCs). Historically, *Azadirachta Indica* leaf (AIL) extract has been recognized as a promising material in the fields of antimicrobial and medicinal applications. AIL/ZnO nanoparticles exhibit significant antimicrobial effects against a broad spectrum of microorganisms. ZnO, in both micro and nano forms, has also been identified as an effective and cost-efficient antimicrobial agent compared to silver (Ag). Therefore, combining small amounts of AIL with relatively inexpensive ZnO nanoparticles offers a strategic approach to enhance both photocatalytic and antimicrobial properties (Ghosh *et al.* 2022). In this study, AIL/ZnO nanoparticles were synthesized using the aqueous extract of *Azadirachta Indica* L. (neem), which acted as both a reducing and stabilizing agent. *Azadirachta Indica* (neem) leaf extract is used in ZnO nanoparticle synthesis to reduce agglomeration, enhance dispersion, and introduce bioactive compounds that act as stabilizers and co-catalysts. This improves surface area, particle size, and electron-hole separation, enhancing photocatalytic and antimicrobial performance. Its eco-friendly synthesis and versatile applications make AIL/ZnO an efficient material for environmental and medical uses. The synthesized AIL/ZnO nanoparticles were tested for their photocatalytic activity in the degradation of Methylene Blue dye. The results demonstrated their effectiveness as a photocatalyst under light exposure. This highlights the potential of AIL/ZnO composites for environmental remediation (Saeed *et al.* 2019).

2. MATERIALS AND METHODS

2.1 Preparation of AIL Extract

The branches of AIL were stripped of their leaves after collection from my locality in Thiruvavur district, Tamil Nadu. To remove dirt and debris, the collected leaves were washed once with tap water and twice with distilled water. After washing, the leaves were air-dried in the shade for one week. The dried leaves were

ground into a fine powder using an electronic grinder and subsequently sieved through a fine-mesh sieve. For the preparation of the plant extract, 1.35 g of the powdered leaves were mixed with 200 mL of distilled water in a 500 mL beaker. The mixture was stirred continuously for two hours on a hot plate. After stirring, the solution was filtered through Whatman No. 40 filter paper, yielding 160 mL of a green-colored plant extract (Fig. 1). The filtrate was further refined using a Buchner funnel and stored for subsequent use (Akhtar *et al.* 2024).

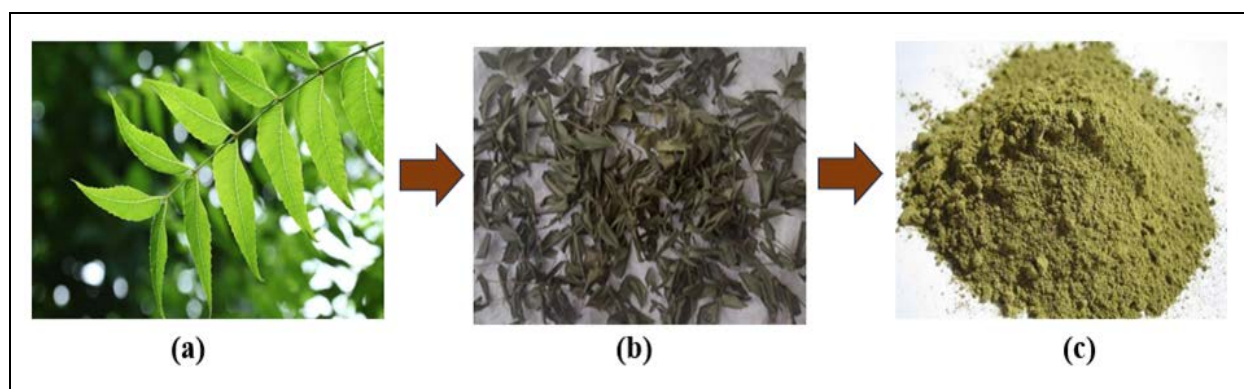


Fig. 1: (a) Green AIL (b) Dried AIL (c) AIL powder

Table 1. Botanical classification of *Azadirachta Indica* (Neem) Leaf

Kingdom	Plantae
Order	Sapindales
Family	Meliaceae
Genus	<i>Azadirachta Indica</i>
Species	<i>Azadirachta Indica</i>
Clade	Angiosperms
Clade	Tracheophytes

2.2 Biosynthesis of ZnO NPs

To synthesize zinc oxide (ZnO) nanoparticles, an aqueous solution of $\text{ZnSO}_4 \cdot 7\text{H}_2\text{O}$ (0.2 M, 50 mL) was mixed with NaOH (2.0 M, 50 mL) in a 250 mL conical flask. Neem extract (20 mL, light green in color) was gradually added dropwise to the $\text{ZnSO}_4 \cdot 7\text{H}_2\text{O}$ solution at room temperature. The pH of the mixture was adjusted to 7, and the solution was stirred continuously for 4 hours at 60 °C. This process yielded a deep green paste, which was then filtered to remove impurities Rani *et al.* (2024). During the reaction, the color transition from light green to pale white suggested the reduction of Zn^{2+} ions to ZnO nanoparticles, confirmed by UV-Vis spectral analysis. The filtrate was then dried at 80 °C in an oven for 12 hours. The resulting paste was transferred to a ceramic crucible and annealed at 500 °C for 3 hours, producing a light white powder (Rani *et al.* 2024). Finally, the powder

was ground into a fine white form using a mortar and pestle and stored for subsequent characterization.

Table 2. Physicochemical Properties and Chemical Structure of Methylene Blue

Physicochemical properties	Description
Molecular formula	$\text{C}_{16}\text{H}_{18}\text{N}_3\text{ClS}$
Molecular weight	319.85 g/mol
Solubility	43.6 g/L in water at 25°C
Color	Deep blue solution in water or alcohol
Chemical Structure	
Melting point	100–110°C

2.3 Photodegradation with Solar Light

Photocatalytic experiments were conducted from March to May 2024, between 10:00 am and 2:00 pm, with sunlight intensity averaging $197.7 \pm 31.8 \text{ W/m}^2$ and temperatures at $31 \pm 2 \text{ }^\circ\text{C}$ to assess nanoparticle efficiency in degrading methylene blue (MB). The photocatalytic degradation efficiency of methylene blue (MB) using AIL/ZnO catalysts under solar light across various conditions is illustrated in Fig. 2. MB dye showed resistance to direct photolysis by solar light alone. A slight reduction in dye concentration (approximately 21%) was observed when MB was treated with AIL/ZnO in dark conditions for 60 minutes. Under irradiation with

ZnO alone in solar light, 58% degradation of MB was achieved within 60 minutes. Notably, among the AIL/ZnO catalysts with varying weight percentages, the catalyst containing 7 wt.% AIL/ZnO demonstrated the highest degradation efficiency of 90% within 60 minutes. Therefore, 7 wt.% AIL/ZnO was identified as the optimal concentration for further studies. Characterization of the 7 wt.% AIL/ZnO catalyst was conducted, and its photocatalytic performance under UV-A and solar light was examined, along with the influence of different process parameters on MB degradation. Table 2 provides the physicochemical properties, maximum absorption wavelength (λ_{max}), and chemical structure of MB, used as a model organic dye in this study (Yadeta *et al.* 2024).

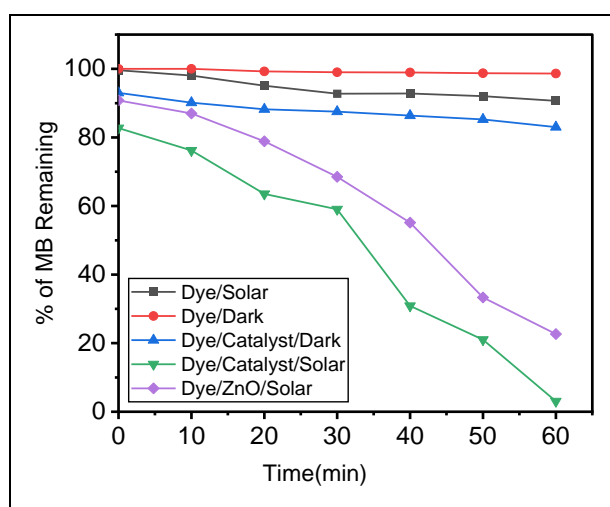


Fig. 2: Primary analysis of AIL/ZnO catalyst with AG-16 under Solar light. [MB] = 4×10^{-4} M, 7 wt% $\text{Ag}_3\text{VO}_4/\text{ZnO}$ = 2 g L^{-1} , airflow rate = 8.1 mL s^{-1} , p^{H} = 7.0, $I_{\text{UV}} = 1.381 \times 10^{-6}$ einstein $\text{L}^{-1} \text{ s}^{-1}$

2.4 Characterization of 7 wt.% of *Azadirachta Indica* Leaf Extract/ZnO Nanocomposites

The morphological and elemental characteristics of AIL/ZnO nanoparticles were investigated using a field emission scanning electron microscope (FEI Quanta FEG200-FESEM) and Bruker Energy Dispersive Spectroscopy (EDS). Crystallographic analysis was conducted with a Benchtop X-ray diffractometer employing Cu-K α radiation ($\lambda = 0.15405 \text{ nm}$) across the Bragg angle range of 2θ (10° – 80°). Surface chemistry was evaluated via X-ray Photoelectron Spectroscopy (XPS) using a PHI 5000 VersaProbe III. Fourier Transform Infrared (FTIR) spectroscopy, equipped with an ATR diamond accessory (IR Tracer 100, AIST/Japan), provided insights into the sample's composition and its influence on performance. Optical properties were examined with a UV-visible Spectrophotometer (UV-2100, Shimadzu).

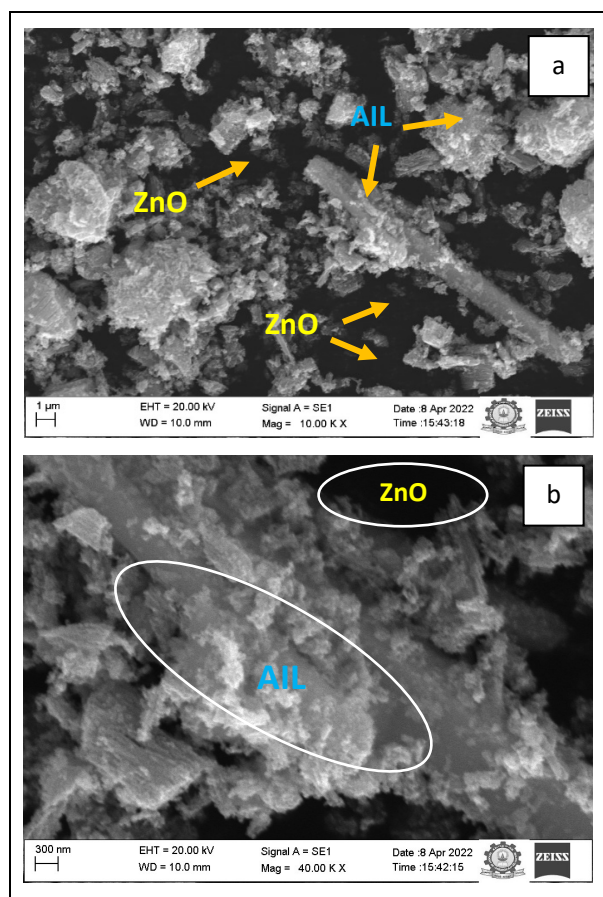


Fig. 3: SEM images of AIL/ZnO nanoparticles and ZnO

3. RESULTS AND DISCUSSIONS

3.1 Morphological Studies

Fig. 3 shows the SEM images of pure ZnO nanoparticles and 7% AIL /ZnO composite nanoparticles, revealing well-dispersed ZnO particles with a crystalline morphology and irregular aggregates. In Fig. 3(a) ZnO appears as dominant, distinct particles, while AIL forms smoother, amorphous regions, likely acting as a capping or stabilizing agent. In Fig. 3(b), the close interaction between ZnO and AIL becomes evident, with AIL coating or bridging ZnO particles, suggesting strong bonding and enhanced integration. This composite structure highlights potential synergistic properties, making it suitable for applications like photocatalysis, antimicrobial coatings, or sensors. The bioextract from AIL likely acts as a stabilizing agent, reducing surface energy and enhancing dispersion by capping the ZnO nanoparticles, thereby limiting particle growth. The presence of bioactive compounds (e.g., flavonoids and polyphenols) in the extract contributes to the reduced particle size and better distribution, as these compounds interact with ZnO precursors during synthesis, preventing excessive aggregation. These morphological changes suggest that the composite nanoparticles have improved stability, increased surface area, and potential

for enhanced catalytic activity compared to pure ZnO. The reduced agglomeration in the composite makes it better suited for applications like photocatalysis, where a higher surface area and uniform particle distribution are advantageous (Kumar *et al.* 2024).

3.2 FTIR Spectroscopic Analysis of Green Synthesized ZnO Nanoparticles

Fourier Transform Infrared (FTIR) spectroscopy (Fig. 4) was used to identify functional groups stabilizing ZnO nanoparticles (NPs) in *Azadirachta Indica* leaf extract (AIL) and its ZnO-doped form. The ZnO spectrum exhibited a characteristic Zn-O stretching vibration ($\sim 450\text{--}500\text{ cm}^{-1}$), confirming pure ZnO without organic interference. The Neem extract showed peaks for O-H stretching ($\sim 3300\text{ cm}^{-1}$, phenols/alcohols), C=C stretching ($\sim 1600\text{ cm}^{-1}$, aromatic flavonoids), and C-O stretching ($\sim 1000\text{--}1100\text{ cm}^{-1}$, esters/alcohols), indicating bioactive organic compounds. In the AIL/ZnO spectrum, shifts in O-H ($\sim 3300\text{ cm}^{-1}$) and C-O ($\sim 1000\text{--}1100\text{ cm}^{-1}$) peaks, along with retention of Zn-O ($\sim 450\text{--}500\text{ cm}^{-1}$), suggest successful functionalization and interaction between ZnO and Neem bio-compounds. These changes confirm the formation of a bio-functionalized ZnO composite, highlighting its potential for use in industrial effluent treatment and related environmental remediation processes.

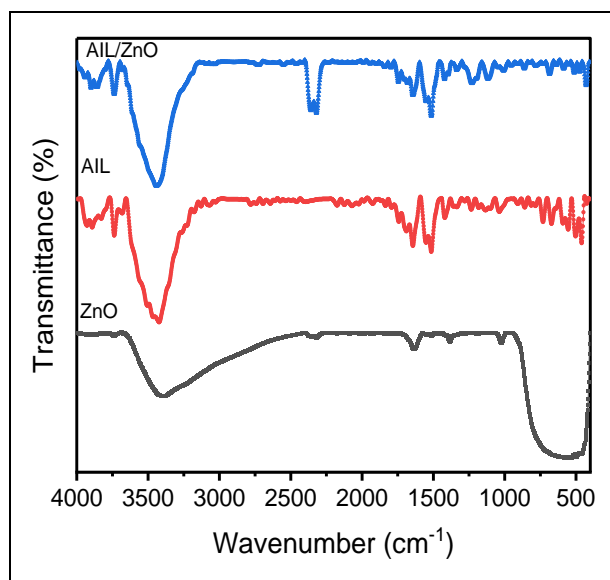


Fig. 4: FTIR Spectrum of AIL/ZnO nanoparticles, AIL and ZnO

3.3 X-Ray Diffraction Analysis of Green Synthesized ZnO NPs

Fig. 5 XRD analysis confirms that ZnO nanoparticles exhibit high crystallinity and purity, maintaining the hexagonal wurtzite structure (JCPDS

#36-1451). Key diffraction peaks at $2\theta = 31.77^\circ$ ($d = 2.814\text{ \AA}$, (100)), 34.42° ($d = 2.603\text{ \AA}$, (002)), and 36.25° ($d = 2.476\text{ \AA}$, (101)) affirm this structural integrity. In contrast, the neem leaf extract shows an amorphous nature, with broad, low-intensity peaks due to its organic biomolecules like polyphenols and flavonoids. The Neem-ZnO composite retains the primary ZnO peaks but with reduced intensity and slight broadening (e.g., $2\theta = 31.68^\circ$, 34.35° , 36.15°). The 2θ values, d-spacing, Relative intensity and plane value are summarized in table 3. The crystalline size of the ZnO nanoparticles synthesized in this study was determined using X-ray Diffraction (XRD) analysis and Scherrer's formula, applied to the prominent peak at 36.33° (101 planes). The calculated average particle size was 16.21 nm. For further confirmation, Transmission Electron Microscopy (TEM) or Scanning Electron Microscopy (SEM) could be used. The XRD analysis confirms the crystalline nature and size of the ZnO nanoparticles. This suggests a successful interaction between ZnO and the neem extract's organic components, leading to structural and surface modifications. These changes enhance the composite's potential for photocatalysis, antibacterial and antimicrobial applications.

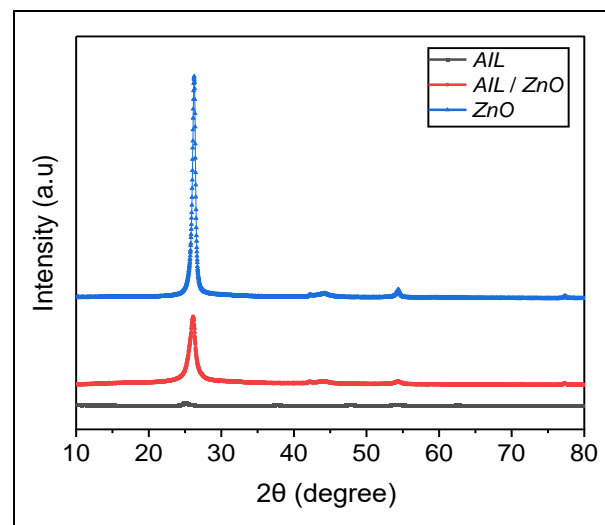


Fig. 5: XRD Spectrum of AIL/ ZnO nanoparticles, AIL and ZnO

3.4 UV-DRS analysis of Green Synthesized ZnO NPs

The UV-DRS analysis of ZnO, *Azadirachta Indica* leaf extract (AIL), and AIL/ZnO (7% AIL-doped ZnO) reveals significant optical property modifications due to doping. Pure ZnO exhibits a band gap energy of 3.23 eV, consistent with its typical semiconductor behavior. The incorporation of AIL reduces the band gap energy to 2.80 eV, attributed to the organic components in the Neem extract introducing impurity levels. For the AIL/ZnO composite, the band gap is further adjusted to 2.95 eV, reflecting a balance between the ZnO matrix and

the dopant's influence. The observed red-shift in the absorption edge for AIL/ZnO indicates enhanced visible light absorption, making it more efficient for photocatalytic applications. Doping with AIL modifies the electronic structure of ZnO by introducing localized states, which facilitate better electron-hole separation and reduce recombination (Rajyashree *et al.* 2024). This narrowing of the band gap enhances light-harvesting capabilities and broadens the material's applicability under solar irradiation. The reduced band gap and enhanced visible light absorption of AIL/ZnO will be linked to improved photocatalytic efficiency. We will calculate and compare the photocatalytic performance of AIL/ZnO with pure ZnO to support our findings. The synergy between AIL and ZnO demonstrates the potential of Neem extract as an eco-friendly dopant to improve photocatalytic efficiency. These results suggest that AIL/ZnO is a promising material for visible light-driven applications, with the reduced band gap energy being a key contributor to its improved performance, as shown in Fig. 6(a) and (b).

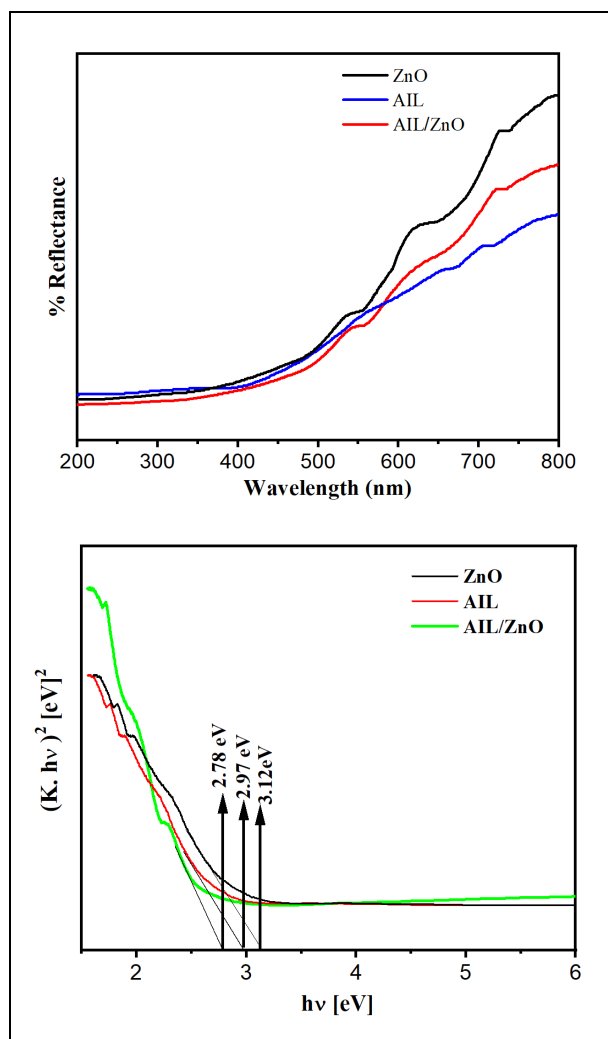


Fig. 6: (a) UV-DRS Spectrum of 7% AIL/ZnO (b) Band gap energy of 7% AIL/ZnO

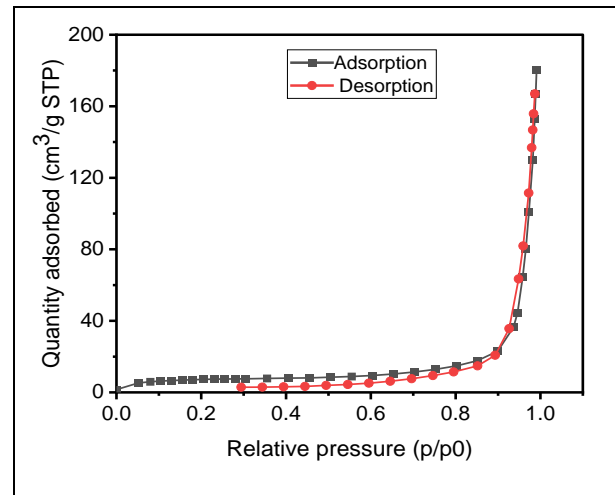


Fig. 7: BET isotherm pattern AIL/ZnO nanocomposites

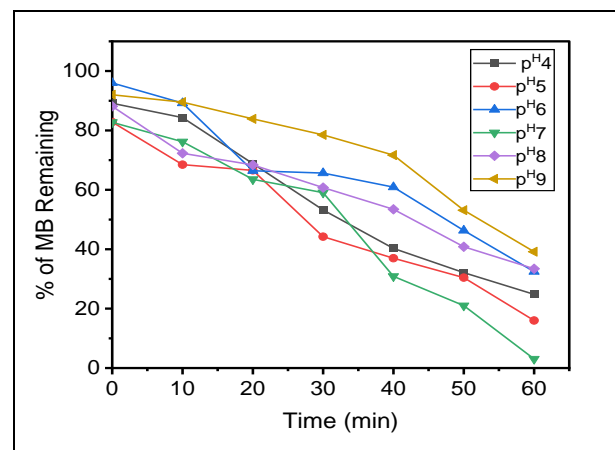


Fig. 8: Effect of pH- Solar (degradation). [MB] = 4×10^{-4} M, 7 wt.% AIL/ZnO = 2 g L^{-1} , airflow rate = 8.1 mL s^{-1} , irradiation time = 30 min, $I_{\text{Solar}} = 1.381 \times 10^{-6} \text{ einstein L}^{-1} \text{ s}^{-1}$

3.5 BET Surface Area

The resultant adsorption-desorption isotherms for N_2 and 7% AIL/ZnO were then subjected to the Brunauer Emmett Teller (BET) analysis, as shown in Fig. 7. The results demonstrated that in accordance with the IUPAC categorization of adsorption isotherms (Thommes *et al.* 2016), the N_2 isotherm is similar to the type II, having a sharp adsorption capacity while indicating the presence of broader pore size distributions, smaller mesopores, and wider micropores. The BET analysis of AIL-doped zinc oxide is anticipated to reveal a greater surface area than any of the individual components alone. This is due to the possibility that adding AIL extract may enhance the number of surface sites available for gas adsorption. The catalyst's surface area and pore structure are the primary variables that influence catalytic activity. Using the nitrogen gas adsorption technique, the surface area of AIL/ZnO was measured. AIL/ZnO samples N_2 gas adsorption/desorption isotherm curve resembles a type II isotherm

curve with a hysteresis loop. To determine the BJH pore size distribution, the desorption isotherm was employed. AIL and ZnO have computed average pore sizes of 33.06 nm and 33.06 nm, respectively. Overall, BET analysis may offer useful information regarding the surface area and porosity of AIL-doped zinc oxide, which can assist in directing its development and possible applications.

3.6 Effect of Experimental Conditions

3.6.1 Effect of pH

Fig. 8 illustrates the impact of pH on the photocatalytic degradation rate of MB using AIL/ZnO, with pH values ranging from 4 to 9. As pH increases from 4 to 7, the degradation rate enhances, reaching its peak at pH 7, indicating the optimal conditions for degradation. The degradation rate varies from 0.007 to 0.014 min⁻¹, with pH 7 yielding the highest rate of 0.014 min⁻¹, as evidenced by the graph showing a consistent reduction in concentration over time (Bairwa *et al.* 2024). However, beyond pH 7, the degradation efficiency declines, as indicated by slower rates at pH 8 and 9. This highlights that pH 7 is optimal, with a significant reduction in photocatalytic activity observed at higher alkaline pH values (8–9).

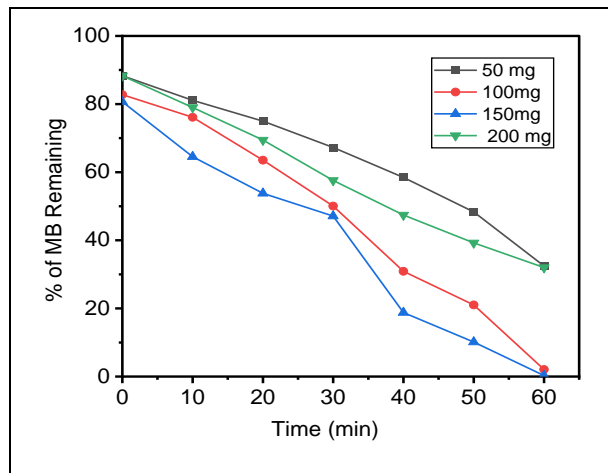


Fig. 9: Effect of Catalyst Loading- Solar (degradation). [MB] = 4×10^{-4} M, 7 wt.% AIL/ZnO = 2 g L^{-1} , airflow rate = 8.1 mL s^{-1} , irradiation time = 30 min, $I_{\text{solar}} = 1.381 \times 10^{-6} \text{ einstein L}^{-1} \text{ s}^{-1}$

3.6.2 Effect of Catalyst Loading

Fig. 9 demonstrates the effect of catalyst loading on the degradation rate of MB using AIL/ZnO. As the catalyst concentration increases from 50 mg to 200 mg, the degradation rate improves, with the highest efficiency observed at 200 mg (green line). This trend aligns with the text, which suggests that increasing catalyst concentration enhances degradation up to an optimal level (Bairwa *et al.* 2024). The degradation rate is lower at 50 mg, while 100 mg and 150 mg show progressively better performance, with 200 mg yielding the highest efficiency. Although the text indicates an optimal catalyst

loading of 3 g L^{-1} , beyond which degradation efficiency declines due to excessive catalyst blocking light and reducing the active surface area, this decline is not reflected in the graph, as the highest efficiency is still achieved at 200 mg.

3.6.3 Effect of Dye Concentration

Fig. 10 demonstrates that lower dye concentrations result in higher degradation rates, with rate constants ranging from 0.046 min^{-1} for 1×10^{-4} M to 0.007 min^{-1} for 5×10^{-4} M. As the dye concentration increases, degradation efficiency decreases, likely due to a reduction in available active sites on the photocatalyst and increased light scattering (Bairwa *et al.* 2024). Therefore, the photocatalytic process is more efficient at lower dye concentrations.

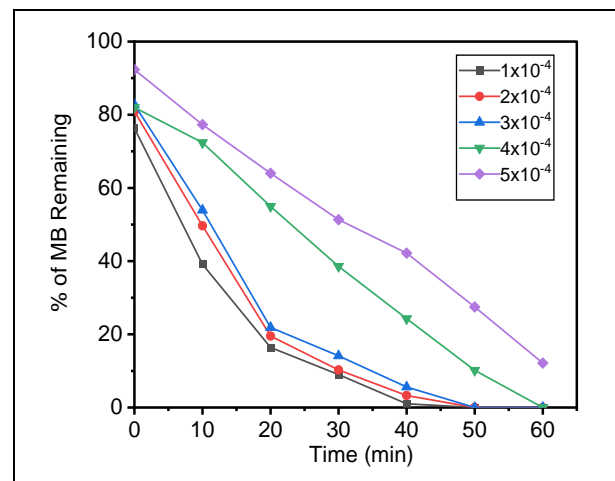


Fig. 10: Effect of Dye Concentration- Solar (degradation). [MB] = 4×10^{-4} M, 7 wt.% AIL/ZnO = 2 g L^{-1} , airflow rate = 8.1 mL s^{-1} , irradiation time = 30 min, $I_{\text{solar}} = 1.381 \times 10^{-6} \text{ einstein L}^{-1} \text{ s}^{-1}$

3.7 Screening of Antimicrobial Activity

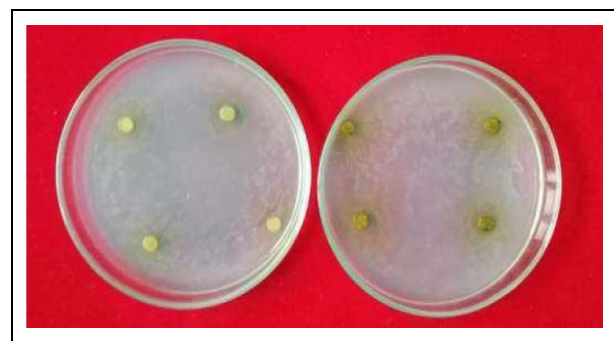


Fig. 11: Antimicrobial activity of 7% AIL/ZnO composite against (a) E. Coli (b) Staphylococcus aureus

Fig. 11 demonstrates the antimicrobial activity of *Azadirachta Indica* (neem) leaf extract doped with ZnO (AIL/ZnO) was evaluated against *Escherichia coli* and *Staphylococcus aureus* using varying concentrations

(50 μL , 100 μL , and 150 μL). The results showed that AIL/ZnO exhibited notable antimicrobial effects, with zones of inhibition increasing with concentration (Table 3). For *E. coli*, the inhibition ranged from 12 mm at 50 μL and 100 μL to 13 mm at 150 μL , surpassing the standard gentamicin (10 mm). For *S. aureus*, the composite showed zones of inhibition from 16 mm at 50 μL and 100 μL to 17 mm at 150 μL , outperforming gentamicin (15 mm). These findings suggest that the synergy between neem's bioactive compounds and ZnO nanoparticles enhances the antimicrobial activity, making AIL/ZnO a promising alternative to conventional antibiotics, with higher effectiveness at elevated concentrations. The results underscore the potential of neem-ZnO composites for broad-spectrum antimicrobial applications.

The antimicrobial activity of *Azadirachta Indica* (neem) leaf extract-doped ZnO nanoparticles (AIL/ZnO) was evaluated against common bacterial strains, including *Escherichia coli* and *Staphylococcus aureus*. The results revealed significant antimicrobial efficacy, with zones of inhibition surpassing those of standard antibiotics like gentamicin. At a concentration of 150 μL , AIL/ZnO exhibited inhibition zones of 13 mm for *E. coli* and 17 mm for *S. aureus*, outperforming gentamicin by 3 mm and 2 mm, respectively.

Table 3. Antimicrobial activity of 7% AIL/ZnO composite

Plants	Microorganism	Zone of Inhibition in mm			
		50 μL	100 μL	150 μL	Standard (Gentamicin)
AIL/ZnO	<i>E. Coli</i>	12	12	13	10
AIL/ZnO	<i>S. aureus</i>	16	16	17	15

3.7.1 Mechanisms of Action

AIL/ZnO demonstrates its antimicrobial potency through: Enhanced ROS Generation: Reactive oxygen species disrupt bacterial membranes, leading to oxidative stress and eventual cell death. The bioactive compounds in neem extract synergize with ZnO to amplify ROS production. Synergistic Effects of Neem Phytochemicals: Compounds such as azadirachtin and quercetin enhance bacterial membrane disruption and DNA fragmentation. Improved Surface Interactions: The doping of ZnO with neem extract results in smaller nanoparticle sizes and increased surface area, facilitating better bacterial interaction.

3.7.2 Comparison with Other Synthesis Approaches

Compared to other green synthesis methods, AIL/ZnO exhibits superior antimicrobial activity due to its phytochemical synergy. For instance, ZnO nanoparticles synthesized using aloe vera or citrus peels demonstrate moderate activity but require higher doses to achieve similar inhibition. Conventional ZnO nanoparticles, while effective, necessitate UV activation

for ROS generation and display reduced activity against resistant strains like MRSA.

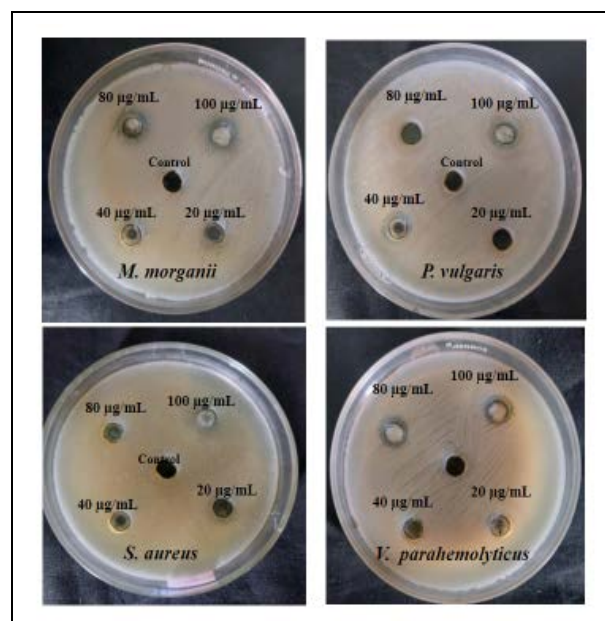


Fig. 12: Antibacterial activity of 7% AIL/ZnO composite against (a) *Morganella morganii* (b) *Proteus vulgaris* (c) *Staphylococcus aureus* and (d) *Vibrio parahaemolyticus*

Table 4. Minimum bactericidal activity

Bacterial Culture Name	Formation of zone of inhibition (mm) at different concentrations of 7% AIL/ZnO sample			
	20 $\mu\text{g/mL}$	40 $\mu\text{g/mL}$	80 $\mu\text{g/mL}$	100 $\mu\text{g/mL}$
<i>Morganella morganii</i>	-	-	2.03 \pm 0.05	3.1 \pm 0.08
<i>Proteus vulgaris</i>	-	3.3 \pm 0.25	5.2 \pm 0.2	6.1 \pm 0.15
<i>Staphylococcus aureus</i>	-	-	1.03 \pm 0.15	2.1 \pm 0.17
<i>Vibrio parahaemolyticus</i>	-	-	2.1 \pm 0.1	3.07 \pm 0.06

3.8 Antibacterial Assay

The *Azadirachta Indica* (neem) leaf extract doped with Zinc oxide (AIL/ZnO) shows promising antibacterial activity, with potential applications in combating bacterial infections (Fig. 12). The catalyst demonstrated concentration-dependent antibacterial effects against *Morganella morganii*, *Proteus vulgaris*, *Staphylococcus aureus*, and *Vibrio parahaemolyticus*. At higher concentrations (80 $\mu\text{g/mL}$ and 100 $\mu\text{g/mL}$), significant inhibition zones were observed, particularly for *Proteus vulgaris*, which exhibited the largest inhibition of 6.1 \pm 0.15 mm at 100 $\mu\text{g/mL}$. Moderate inhibition was noted for *Vibrio parahaemolyticus* (3.07 \pm 0.06 mm) and *Staphylococcus aureus* (2.1 \pm 0.17 mm) at 100 $\mu\text{g/mL}$, indicating the broad-spectrum potential of the composite (Table 4). The catalyst showed minimal activity at lower concentrations, suggesting that higher

doses of AIL/ZnO are necessary for effective antibacterial action. These findings highlight the catalyst's potential for use in antibacterial coatings, wound dressings, or as an antimicrobial agent in medical and environmental applications. The enhanced activity of AIL/ZnO against Gram-negative bacteria like *Proteus vulgaris* positions it as a promising alternative to conventional antibiotics, especially in the treatment of resistant bacterial strains.

3.9 Photocatalytic Mechanism

The mechanism of *Azadirachta Indica* (neem) leaf extract doped with Zinc oxide (ZnO) for the photocatalytic degradation of Methylene Blue (MB) dye under solar light involves several steps (Fig. 13). ZnO acts as a semiconductor, and under solar light, it absorbs photons with energy greater than or equal to its bandgap (approximately 3.37 eV for ZnO). This absorption generates electron-hole pairs (e^-/h^+) at the surface of ZnO. The energy of the absorbed light excites electrons from the valence band to the conduction band, leaving behind holes in the valence band. The electron in the conduction band (e^-) can be captured by O_2 molecules adsorbed on the ZnO surface, forming superoxide radicals ($O_2^{\cdot-}$). The hole in the valence band (h^+) can react with H_2O or OH^- ions adsorbed on the surface, generating hydroxyl radicals ($\cdot OH$). The neem leaf extract plays a crucial role in enhancing the photocatalytic efficiency by acting as a stabilizing agent and co-catalyst. Active compounds like flavonoids, alkaloids, and tannins in the neem extract can act as electron donors, donating electrons to the conduction band of ZnO and reducing electron-hole recombination. These compounds also help

in surface modification of ZnO, leading to improved adsorption of the dye molecules and better interaction between ZnO and MB dye. The $O_2^{\cdot-}$ and $\cdot OH$ radicals are highly reactive species that degrade organic pollutants such as Methylene Blue (MB). These radicals attack the MB dye molecules, breaking the chemical bonds in the dye structure, leading to decolorization and mineralization of the dye into smaller, less harmful molecules. The presence of ZnO enhances the photocatalytic activity by providing a semiconductor surface for dye adsorption and radical formation. ZnO also contributes to better electron-hole separation, improving the overall efficiency of the degradation reaction. The Bandgap Energy of ZnO 3.37 eV. The Solar intensity light ranges from 1000 W/m² under full sunlight. Degradation studies range from 10mg/L. The rate of photodegradation ranges from 60 to 99% within 60 minutes with the optimum pH of 7-9. The neem leaf extract doped with ZnO acts as a synergistic photocatalyst, improving the photocatalytic degradation of methylene blue dye under solar light. The combination of solar photon absorption, radical formation, and surface modification by neem extract leads to efficient dye degradation, with high rates of decolorization and mineralization of the dye.

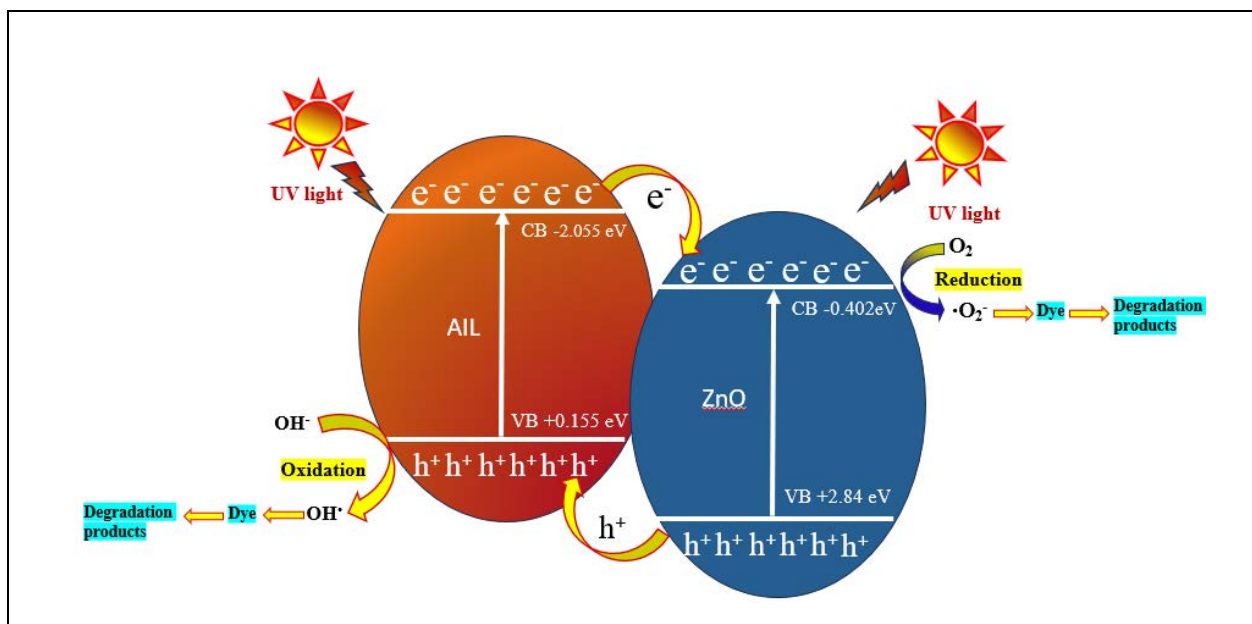
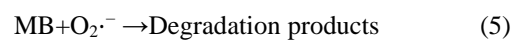
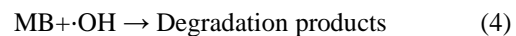
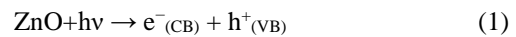


Fig. 13: Schematic diagram of AIL/ZnO nanocomposite mechanism of dye degradation

4. CONCLUSION

The *Azadirachta Indica* (neem) leaf extract doped with ZnO (AIL/ZnO) demonstrates significant enhancements in structural, surface, and functional properties, making it a promising material for diverse applications. The incorporation of neem extract reduces agglomeration, improves dispersion, and introduces bioactive compounds that act as stabilizing agents and co-catalysts. The novelty of this work lies in using *Azadirachta Indica* (neem) leaf extract as both a reducing and stabilizing agent for ZnO nanoparticle synthesis, avoiding toxic chemicals. Neem's phytochemicals enhance nanoparticle stability and biocompatibility. The approach achieves 100% dye degradation in under 22 minutes and exhibits strong antimicrobial properties, offering a sustainable, cost-effective alternative to traditional methods. These modifications lead to increased surface area, better particle size distribution, and efficient electron-hole pair separation, which are critical for advanced applications. AIL/ZnO composites exhibit superior photocatalytic activity, achieving a degradation rate of 60–99% for methylene blue under optimal conditions (pH 7, 10 mg/L dye concentration, and 200 mg catalyst loading). This is attributed to synergistic interactions between ZnO and neem bio-compounds, enabling efficient radical generation and dye mineralization. Beyond photocatalysis, AIL/ZnO holds potential in environmental remediation, including wastewater treatment and degradation of other organic pollutants. The enhanced antimicrobial properties against bacteria such as *E. coli* and *S. aureus* highlight its utility in medical applications like antibacterial coatings, wound dressings, and sterilization tools. Furthermore, its role in solar-driven processes opens pathways for renewable energy utilization in sustainable technologies. Overall, the combination of green synthesis, multifunctional capabilities, and environmentally friendly operations positions AIL/ZnO composites as versatile materials for addressing industrial and environmental challenges.

FUNDING

This research received no specific grant from any funding agency in the public, commercial, or not-for-profit sectors.

CONFLICTS OF INTEREST

The authors declare that there is no conflict of interest.

COPYRIGHT

This article is an open-access article distributed under the terms and conditions of the Creative Commons

Attribution (CC BY) license
(<http://creativecommons.org/licenses/by/4.0/>).



REFERENCES

- Akhtar, M. S., Fiaz, S., Aslam, S., Chung, S., Ditta, A., Irshad, M. A., Al-Mohaimed, A. M., Iqbal, R., Al-onazi, W. A., Rizwan, M. and Nakashima, Y., Green synthesis of magnetite iron oxide nanoparticles using *Azadirachta Indica* leaf extract loaded on reduced graphene oxide and degradation of methylene blue, *Sci. Rep.*, 14(1), 18172 (2024).
<https://doi.org/10.1038/s41598-024-69184-y>
- Algarni, T. S., Abduh, N. A. Y., Aouissi, A. and Al Kahtani, A., Photodegradation of methyl orange under solar irradiation on Fe-doped ZnO nanoparticles synthesized using wild olive leaf extract, *Green Process. Synth.*, 11(1), 895–906 (2022).
<https://doi.org/10.1515/gps-2022-0077>
- Alqarni, L. S., Alghamdi, M. D., Alshahrani, A. A. and Nassar, A. M., Green Nanotechnology: Recent Research on Bioresource-Based Nanoparticle Synthesis and Applications, *J. Chem.*, 2022, 1–31 (2022).
<https://doi.org/10.1155/2022/4030999>
- Ashour, M., Mansour, A. T., Abdelwahab, A. M. and Alprol, A. E., Metal Oxide Nanoparticles' Green Synthesis by Plants: Prospects in Phyto- and Bioremediation and Photocatalytic Degradation of Organic Pollutants, *Processes*, 11(12), 3356 (2023).
<https://doi.org/10.3390/pr11123356>
- Bairwa, P. and Devra, V., Plant-mediated bimetallic nanoparticles synthesis for catalytic degradation of malachite green, *Acad Eng.*, 1(3), (2024).
<https://doi.org/10.20935/AcadEng7320>
- Ghosh, T., Chattopadhyay, A., Pramanik, S., Das, A., Mukherjee, S., Das, S., Mandal, A. C., Dhak, D. and Kuiri, P. K., Role of Ag Nanoparticles on Photoluminescence Emissions, Antibacterial Activities, and Photocatalytic Effects in ZnO-Ag Nanocomposites Synthesized via Low Temperature Green Synthesis Method Using *Azadirachta Indica* Leaf Extract, *Mater. Technol.*, 37(12), 2300–2312 (2022).
<https://doi.org/10.1080/10667857.2022.2029290>
- Hessien, M., Da'na, E. and Taha, A., Phytoextract assisted hydrothermal synthesis of ZnO–NiO nanocomposites using neem leaves extract, *Ceram. Int.*, 47(1), 811–816 (2021).
<https://doi.org/10.1016/j.ceramint.2020.08.192>

- Karvekar, O. S., Sarvalkar, P. D., Vadanagekar, A. S., Singhan, R. D., Jadhav, S. M., Nimbalkar, M. S. and Prasad, N. R., Biogenic synthesis of silver anchored ZnO nanorods as nano catalyst for organic transformation reactions and dye degradation, *Appl. Nanosci.*, 12(7), 2207–2226 (2022). <https://doi.org/10.1007/s13204-022-02470-1>
- Kavya, P., K. M. and Prakash, V., Synthesis and characterization of MgO nanoparticles using chemical reducing agents and leaf extract of neem, *Mater Today Proc.*, (2023). <https://doi.org/10.1016/j.matpr.2023.04.282>
- Kumar, N., Rathore, A. and Devra, V., Green synthesis of metal nanoparticles and their applications in degradation of azo dye, *Acad Eng.*, 1(2), (2024). <https://doi.org/10.20935/AcadEng6211>
- Martin, M. M., Sumayao, Jr., R. E., Soriano, A. N. and Rubi, R. V. C., Photocatalytic Degradation Activity of the Biosynthesized *R. rosifolius* Mediated Silver Nanoparticles in Methylene Blue Dye, *Asean J. Chem. Eng.*, 23(3), 329 (2023). <https://doi.org/10.22146/ajche.82506>
- Oza, G., Reyes-Calderón, A., Mewada, A., Arriaga, L. G., Cabrera, G. B., Luna, D. E., Iqbal, H. M. N., Sharon, M. and Sharma, A., Plant-based metal and metal alloy nanoparticle synthesis: a comprehensive mechanistic approach, *J. Mater. Sci.*, 55(4), 1309–1330 (2020). <https://doi.org/10.1007/s10853-019-04121-3>
- Qasim, M., Arif, M. I., Naseer, A., Ali, L., Aslam, R., Abbasi, S. A., Qamar, M. S. and Ullah, Q., Biogenic Nanoparticles at the Forefront: Transforming Industrial Wastewater Treatment with TiO₂ and Graphene, *Sch. J. Agric. Vet. Sci.*, 11(05), 56–76 (2024). <https://doi.org/10.36347/sjavs.2024.v11i05.002>
- Rajyashree, L., Manoharan, C., Loganathan, A., Venkateshwarlu, M. and SanjayKumar Arasumani, The effect of reaction temperature on structural and morphological properties of Mn₂O₃ nanoparticles and its application of electrochemical and gas sensor, *Mater. Technol.*, 37(14), 3051–3062 (2024). <https://doi.org/10.1080/10667857.2022.2119680>
- Rani, N., Yadav, S., Mushtaq, A., Rani, S., Saini, M., Rawat, S., Gupta, K., Saini, K. and Maity, D., *Azadirachta Indica* peel extract-mediated synthesis of ZnO nanoparticles for antimicrobial, supercapacitor and photocatalytic applications, *Chem. Pap.*, 78(6), 3687–3704 (2024). <https://doi.org/10.1007/s11696-024-03340-6>
- Ravikumar, A. and Prakash, K. S., Green and Sustainable Approaches of Nanoparticles, In: Handbook of Consumer Nanoproducts, *Springer Nature*, 1433–1453 (2021). https://doi.org/10.1007/978-981-15-6453-6_81-1
- Rekha, S., Jagadheeswari, Arunprasath and Sumathy, Durability properties of copper slag and fly ash based concrete for a sustainable environment, *Mater. Today Proc.*, 37, 2535–2541 (2021). <https://doi.org/10.1016/j.matpr.2020.08.490>
- Saeed, M., Muneer, M., Khosa, M. K. K., Akram, N., Khalid, S., Adeel, M., Nisar, A. and Sherazi, S., *Azadirachta Indica* leaves extract assisted green synthesis of Ag-TiO₂ for degradation of Methylene blue and Rhodamine B dyes in aqueous medium, *Green Process. Synth.*, 8(1), 659–666 (2019). <https://doi.org/10.1515/gps-2019-0036>
- Sahin, M. and Gubbuk, I. H., Green synthesis of palladium nanoparticles and investigation of their catalytic activity for methylene blue, methyl orange and rhodamine B degradation by sodium borohydride, *React. Kinet. Mech. Catal.*, 135(2), 999–1010 (2022). <https://doi.org/10.1007/s11144-022-02185-y>
- Soltys, L., Olkhovyy, O., Tatarchuk, T. and Naushad, M., Green Synthesis of Metal and Metal Oxide Nanoparticles: Principles of Green Chemistry and Raw Materials, *Magnetochemistry*, 7(11), 145 (2021). <https://doi.org/10.3390/magnetochemistry7110145>
- Thommes, M., Physisorption of gases, with special reference to the evaluation of surface area and pore size distribution (IUPAC Technical Report), *Chem. Int.*, 38(1), 25–25 (2016). <https://doi.org/10.1515/ci-2016-0119>
- Yadeta, G. L. and Lealem, B. A., Green synthesis of ZnO, CuO and NiO nanoparticles using Neem leaf extract and comparing their photocatalytic activity under solar irradiation, *Green Chem, Lett, Rev.*, 17(1), (2024). <https://doi.org/10.1080/17518253.2023.2293841>